Ultrasound Elastography - Enabling Technology for Image Guided Laparoscopic Prostatectomy

Ioana N. Fleming[a], Hassan Rivaz[a], Katarzyna Macura[b], Li-Ming Su[c], Ulrike Hamper[b], Gwen A. Lagoda[b], Arthur L. Burnett II[b], Tamara Lotan[b], Russell H. Taylor[a], Gregory D. Hager[a] and Emad M. Boctor[b]

[a]Johns Hopkins University, Baltimore, MD;
[b]Johns Hopkins Medical Institutions, Baltimore, MD.;
[c] University of Florida College of Medicine, Gainesville, FL;

ABSTRACT

Radical prostatectomy using the laparoscopic and robot-assisted approach lacks tactile feedback. Without palpation, the surgeon needs an affordable imaging technology which can be easily incorporated into the laparoscopic surgical procedure, allowing for precise real time intraoperative tumor localization that will guide the extent of surgical resection. Ultrasound elastography (USE) is a novel ultrasound imaging technology that can detect differences in tissue density or stiffness based on tissue deformation. USE was evaluated here as an enabling technology for image guided laparoscopic prostatectomy. USE using a 2D Dynamic Programming (DP) algorithm was applied on data from *ex vivo* human prostate specimens. It proved consistent in identification of lesions; hard and soft, malignant and benign, located in the prostate's central gland or in the peripheral zone. We noticed the 2D DP method was able to generate low-noise elastograms using two frames belonging to the same compression or relaxation part of the palpation excitation, even at compression rates up to 10%. Good preliminary results were validated by pathology findings, and also by *in vivo* and *ex vivo* MR imaging. We also evaluated the use of ultrasound elastography for imaging cavernous nerves; here we present data from animal model experiments.

Keywords: ultrasound, elastography, laparoscopic prostatectomy, prostate, cavernous nerves, nerve imaging

1. INTRODUCTION

Prostate cancer is the second leading cause of cancer death and the most common cancer detected in men in the United States. During 2007 an estimated 218,900 new cases of prostate cancer were diagnosed in the United States, and approximately 27,050 men died of prostate cancer during the same year.[1] Mortality rates have been declining since the mid-1990s, as great strides have been made in both diagnosis and treatment; physicians are able to screen today more patients and therefore detect prostate cancer in their early stages, which are largely cured by surgical intervention. Radical prostatectomy (RP), the modality of treatment which has been shown to improve cancer survival,[2] is a surgical procedure with a goal of complete cancer resection, thus theoretically eliminating the chance for recurrence. Open radical prostatectomies are associated with loss of blood and lengthy recovery times. Laparoscopic radical prostatectomies (LRP) on the other hand, have a very steep learning curve, lack 3-D visualization and use rigid, stick-like instruments which hinder the dissection.

A third technique has recently emerged; laparoscopy using the daVinci Surgical System (Intuitive Surgical, Sunnyvale, CA). The surgical robot introduces many benefits, including three-dimensional visualization, higher magnification, hand tremor elimination and refined dexterity by incorporating wristed instrumentation. Robotic-assisted laparoscopic prostatectomy (RALP) strives to maximize tumor resection and nerve preservation and it is rapidly becoming the preferred surgical approach. The percentage of RPs performed with robotic assistance is increasing as growing numbers of patients diagnosed with clinically localized prostate cancer allow the standardization of this surgical procedure. In 2005, approximately 8000 prostate glands were removed robotically;

Further author information: (Send correspondence to Ioana Fleming)
Ioana Fleming: E-mail: inicola1@jhu.edu, Telephone: 1 410 516 8609

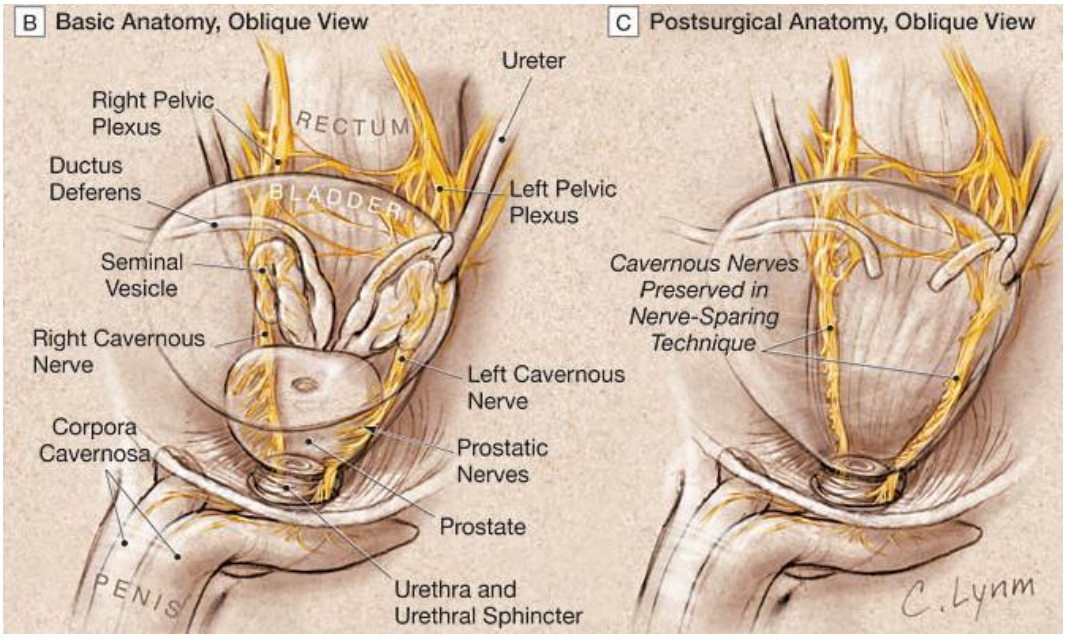

Figure 1. Schematic of the Cavernous Nerves and their preservation during radical prostatectomy; oblique view of male pelvis anatomy, before and after nerve-sparing radical prostatectomy. (Courtesy of Dr. A. L. Burnett, American Medical Association and C. Lynm, 2005)

this number representing more than 10% of all RPs performed that year. In 2007, this number was expected by some to reach 50,000.[3] Systematic reviews from the last 2 (two) years[4,5] have found that RALP is a feasible procedure with a short learning curve, limited blood loss, less post-operative pain, favorable complication rates, and short hospital stay. The lack of tactile feedback is however, one theoretical disadvantage that has been raised with regards to robotic surgery. In open radical prostatectomy, manual palpation is the gold standard in tumor detection.[6] The surgeon feels the periphery of the prostate gland with his or her fingers. Without tactile feedback, a robotic surgeon is unable to appreciate differences in tissue texture or firmness along the prostate surface and therefore may not be able to tailor the extent of tissue excision around the cancerous prostate gland. The inability to identify intra-operatively the cancerous lesions can result in a positive surgical margin (PSM) which is highly associated with cancer recurrence. PSM rates were initially higher in RALP than in the open procedure but they have been shown to decrease in RALP with surgeon's experience and perfected technique.[4] Improvements in robotic tactile or haptic feedback are underway world-wide but are not currently available for clinical use.

There is a need for real-time intraoperative guidance in laparoscopic prostatectomies. Imaging modalities like MRI or CT are not feasible intraoperatively. Transrectal ultrasound (TRUS) is routinely used in prostate cancer diagnostic, in conjunction with digital rectal examination and biopsies. One center reported recently[7,8] their attempt to use real-time TRUS for monitoring and guidance during LRP. The authors reported technical feasibility and enhanced precision proven by decreased rates of PSMs in their center. TRUS was capable of imaging a substantial percent of nonpalpable prostate cancers. The authors recognized however, the limitations of real-time TRUS guidance; it requires considerable prior expertise and tends to identify primarily hypoechoic lesions, which were just 47% of the cancer nodules studied.[8] Recent prostate cancer patients are more likely to present with echogenic or isoechoic lesions because of a shift toward smaller, early-stage cancers;[9,10] classic B-mode gray-scale US alone cannot identify these lesions.

Real-time intraoperative imaging guidance is needed for identifying not only the contours of the tumor but also the precise anatomic course of the cavernous nerves with respect to the underlying prostatic tissue (Figure 1). The cavernous nerves travel along the posterior-lateral wall of the prostate gland within the neurovascular bundle (NVB). Their course runs along the posterior aspect of the prostate. The two distinct areas from which

prostatic nerves leave the gland are thought to be the superior and inferior pedicles; these are the first sites of extra-prostatic spread of cancer. The nervous endings are very small and their trajectory varies from patient to patient making them hard to identify even in the open procedure.[11] Nerves could be spared if no cancer is detected adjacent to them, thus preserving potency, a desirable outcome.[12] Results are mixed or there is still insufficient data with regard to recovery of erectile function from RALP as compared to open prostatectomy.[4] Using TRUS and color Doppler ultrasonography (CDUS), Ukimura et al[7,8] attempted to spare the cavernous nerves. CDUS was helpful in identifying the blood vessels of the NVB; the authors were however unable to identify the nerves so they operated under the principle introduced by Lepor et al[13] that cavernous nerves are usually situated lateral to the vessels, inside the bundle. An imaging technology is needed which is able to visualize the cavernous nerves, thus guiding the surgeon to more appropriate nerve-sparing resection planes.

Elastography is a novel ultrasound imaging technology that can detect differences in tissue density or stiffness based on tissue deformity. Attempts have been made to evaluate the use of elastography for prostate tumor detection using a transrectal ultrasound (TRUS) transducer with promising results.[14] A laparoscopic ultrasound (LUS) probe integrated with the Da Vinci robot was recently used for image guided hepatic cancer surgery,[15] encouraging us to pursue a similar avenue for laparoscopic (robotic) prostatectomy. Integrating elastography technology with a LUS probe will give the surgeons the imaging modality so far missing. This paper describes the experimental design and preliminary results of an ongoing study evaluating the diagnostic accuracy and efficacy of using ultrasound elastography to identify the number and precise sites of cancerous nodules at the surface of the prostate gland, through direct contact with the *ex vivo* specimen. We also present preliminary results from a study attempting to image cavernous nerves in an animal model using ultrasoundelastography.

2. ULTRASOUND ELASTOGRAPHY

Elastography, the computation of the spatial variation of elastic modulus of tissue, is an emerging medical imaging method with various medical applications such as tumor detection.[16] Researchers usually acquire RF-mode ultrasound data from a tissue in both rested and stressed states, estimate the induced strain distribution by tracking speckle motion, and finally produce a first order estimate of the Young's modulus sufficient to describe the elastic properties of (practically uncompressible) soft tissues. Estimating the local strain is the critical step which requires a high level of accuracy, since the amplitude of tissue deformation is small. In[17] small displacements between ultrasonic image pairs which were acquired under a varying axial deformation of the tissue translate into estimates of local displacements of tissue based on correlation analysis of radiofrequency (RF) echoes. Other groups have used iterative phase-based deformation estimation methods[18].[19]

Pellot-Barakat et al.[20] have proposed minimizing an energy function that combines constraints of conservation of echo amplitude and displacement continuity. Here we briefly review the 2D strain imaging technique based on minimizing a similar cost function using Dynamic Programming (DP) for image matching.[21,22] DP has been cited as an efficient non-iterative method for global optimization.[23]

2.1 2D displacement estimation

Two echo signals $g(i)$ and $g'(i)$ corresponding to two A-lines acquired before and after compression are considered, each signal sampled at $i = 1,\ 2 \cdots m$. For ultrasound images consisting of n A-lines, the distance between the pre and post compression signals Δ, can be quantified using sum of absolute differences (SAD):

$$\Delta(i, j, d_a, d_l) = \left| g_j(i) - g'_{j+d_l}(i + d_a) \right| \tag{1}$$

where $d_{a,min} \leq d_a \leq d_{a,max}$ and $d_{l,min} \leq d_l \leq d_{l,max}$ are the axial and lateral displacements respectively at sample i of the j^{th} A-line, $i = 1 \cdots m$, $i = 1 \cdots n$ and d_{min} and d_{max} specify the allowed displacement. The smoothness of the displacements is S

$$S(d_{a_i}, d_{l_i}, d_{a_{i-1}}, d_{l_{i-1}}) = (d_{a_i} - d_{a_{i-1}})^2 + (d_{l_i} - d_{l_{i-1}})^2 \tag{2}$$

The cost function at the ith sample of the jth A-line, and the associated axial and lateral displacements d_a, d_l are

$$\begin{aligned} C_j(d_a, d_l, i) = & \min_{\delta_a, \delta_l} \left\{ \frac{C_j(\delta_a, \delta_l, i-1) + C_{j-1}(\delta_a, \delta_l, i)}{2} + wS(d_a, d_l, \delta_a, \delta_l) \right\} \\ + & \Delta(d_a, d_l, i) \end{aligned} \tag{3}$$

where w is a regularization weight for smoothness. δ_a and δ_l values that minimize eqn. (3) are stored for memoization, for all d_a, d_l and i values. The cost function of the jth line, $C_j(d_a, d_l, i)$, is calculated and is minimized, resulting in its displacement map. The $C_j(d_a, d_l, i)$ function is then used for the calculation of the next cost function $C_{j+1}(d_a, d_l, i)$ and is deleted from the memory afterwards. This makes the amount of memory required to store the cost function values independent of the number of A-lines. Further speed-up is achieved through a hierarchical search; typical runtime is less than 1 second which recommends this method for real-time elastography.[21]

2.2 DP Results

For experimental evaluation we palpated a breast elastography phantom (CIRS, Norfolk, VA) with a lesion of 10mm diameter and three times stiffer than the background. RF data was acquired from an Antares Siemens system (Issaquah, WA) with a 7.27MHz linear array at a sampling rate of 40MHz. Strain images were also calculated using the 1D and 2D DP technique. Signal to noise ratio (SNR) and contrast to noise ratio (CNR) were calculated according to Ophir et al.[17]

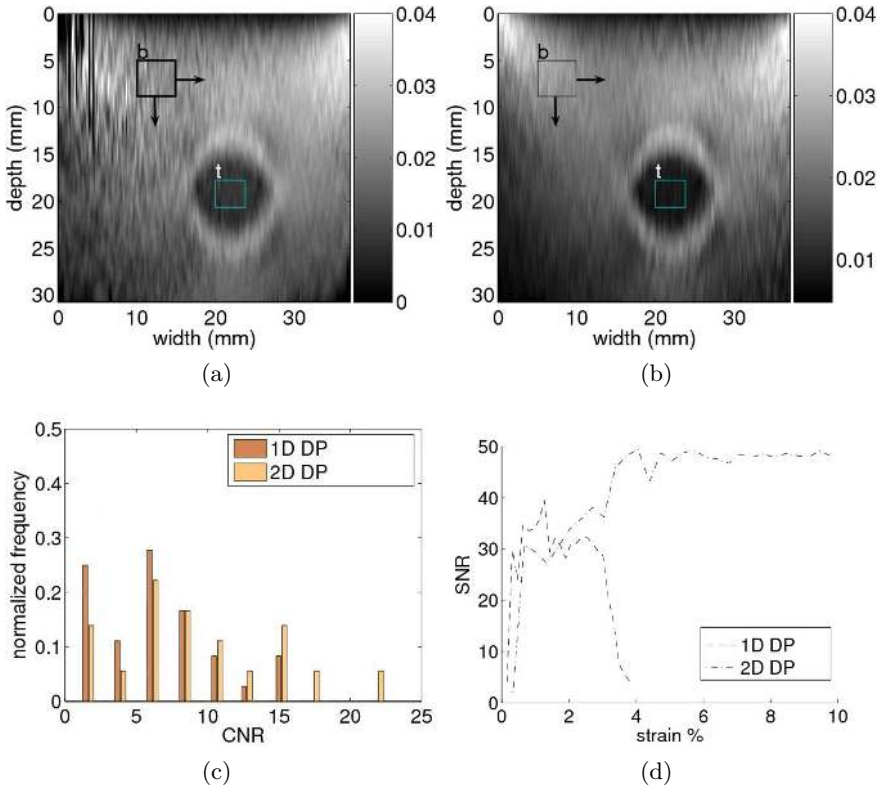

Figure 2. (a)-(b) Strain images from phantom freehand palpation using 1D and 2D DP respectively. The target window is fixed on the lesion and the background window is moved to allow multiple CNR calculation. (c) Normalized CNR values of the lesion, obtained by dividing each bin by the total of 36 CNR measurements. (d) SNR values of for the DP techniques.

In consecutive images the DP methods perform well, even as the axial compression and attendant non-axial motion increase. The histogram of Figure 2 (c) shows CNR values for both DP methods. The SNR metric was calculated in a small window located at the top center of the image, where strain is approximately constant. Figure 2 (d) shows that the DP methods have high dynamic range, an important elastography performance metric.[17]

3. EXPERIMENTAL DESIGN

Patients diagnosed with prostate cancer and candidates for prostatectomy were prospectively enrolled into our study, following an informed consent approved by the Institutional Review Board. One of the objectives of our study is to evaluate the diagnostic accuracy and efficacy of using elastography to identify and precisely localize cancer nodules of the surface of the prostate gland. Patients enrolled in our study undergo pre-operative MRI at 3 Tesla magnetic field strength. Once the prostate is surgically removed (by robotic prostatectomy procedure) the specimen is evaluated *ex-vivo* at ultra high-resolution MRI at 9.4 Tesla to correlate the results to *in-vivo* pre-operative imaging. Ultrasound elastography is then performed by an experienced radiologist blinded to the surgeon's findings or pathology report. Two elastography methods are used: Siemens Antares $eSieTouch^{TM}$ Elasticity Imaging (EI) module online and our DP elastography method offline, using collected RF data. Finally, each prostate specimen undergoes routine pathologic processing and analysis with the histologic findings serving as the "gold standard" to determine the presence and location of any cancerous nodules along the prostate surface. The accuracy and efficacy of elastography is therefore determined by comparison first with the histologic findings noted by the pathologist and then also with both *in-vivo* and *ex-vivo* MRI findings. The size of suspicious nodules on elastography is compared to the histologically determined size of cancerous nodules and MRI. Our results are based on analysis of N=9 target areas in the prostate gland from N=6 patients enrolled so far into the elastography analysis arm.

For our animal experiment, adult male Sprague-Dawley rats (Charles River Breeding Laboratories, Wilmington, MA, USA) weighing 300-350 grams were used. All experiments were conducted in accordance with the Johns Hopkins University School of Medicine guidelines for animal care and use. Animals were anesthetized with an intraperitoneal injection of a mixture of ketamine (100 mg/kg) and xylazine (10 mg/kg). The rats were secured in the supine position while the prostate was exposed via a midline abdominal incision. The cavernous nerves arising from each major pelvic ganglion situated dorsolateral to the prostate was identified and exposed (Figure 7). Ultrasound elastography was performed using the same two methods as in the prostae study. Additional Color Doppler data was collected for verification purposes. At the completion of the study, the rats were euthanized by intracardiac injection of potassium chloride while under anesthesia, consistent with the recommendations of the Panel of Euthanasia of the American Veterinary Medical Association. We report results from imaging N=6 cavernous nerves isolated from N=4 animal subjects.

4. RESULTS AND DISCUSSION

4.1 *Ex-vivo* Human Prostate Experiment

Ultrasound B-mode, RF and elastography data were recorded in freshly resected human prostate specimens. RF acquisition was conducted using a Siemens Antares US scanner (Siemens Medical Solutions USA, Inc. Ultrasound Division, Issaquah, WA) with an ultrasound research interface (URI) to access raw RF data. A Siemens VF 10-5 linear array was used to acquire data using manual handling.

Table 1. Prostate specimen data: A total of 8 (eight) elastography lesions were identified in 5 (five) patients specimens (6 malignant and 2 benign). PZ = peripheral zone, CG = central gland

Specimen Number	Elastography Lesion	Malignant	Location	Size (cm)		
				Elastography	Pathology	MRI
1	1	Yes	PZ base	1.4 x 0.8	1.3 x 0.8	1.3 x 1.1
1	2	No - Solid	CG base	0.7 x 1.1	1.0 x 1.0	1.0 x 1.1
1	3	No - Soft	CG base	1.1 x 0.8	1.0 x 1.0	1.0 x 0.9
2	1	Yes	PZ base	3.0 x 1.3	2.4 x 1.0	2.0 x 1.5
3	1	Yes	PZ mid	2.4 x 0.8	1.9 x 1.0	1.5 x 1.2
4	1	Yes	PZ apex	0.5 x 0.6	0.5 x 0.5	
4	2	Yes	PZ apex	0.6 x 1.0	0.8 x 0.9	
5	1	Yes	PZ base	0.7 x 1.2	0.7 x 1.8	

Freehand palpation was performed on each resected prostate specimen. We used a controlled data collection procedure to facilitate comparison with pathology diagrams. The specimen was scanned both in the prone and

supine position, and data was acquired in multiple transverse scans, from the base of the prostate towards the apex. RF data was used to generate strain images by the 2D DP method. Quantitative data was gathered about the detected lesions for each scan and then compared to pathology report and final tumor mapping on prostate diagrams recording the presence of cancer on transverse sections obtained every 3 mm from the apex to prostate base. Lesion registration was performed by matching areas of high strain on elastography with the corresponding transverse diagram (base, midline, apex) from the pathology report. Data was also compared with *in-vivo* and *ex-vivo* MRI scans.

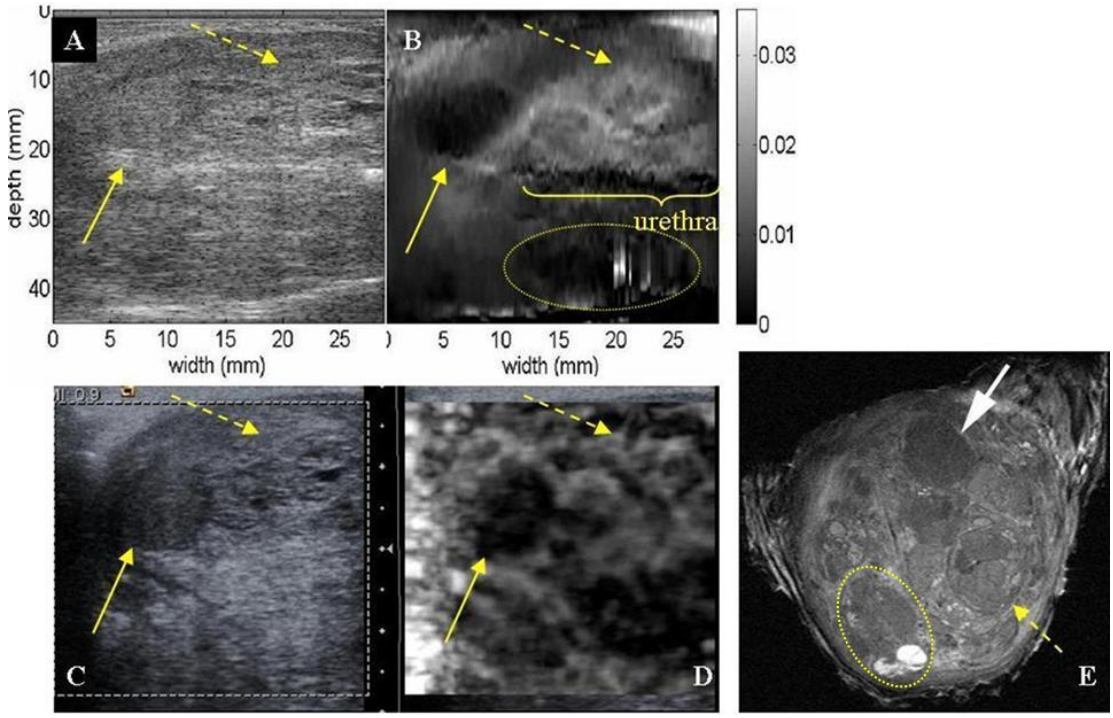

Figure 3. Coronal section of prostate specimen #1. (A) B-mode and (B) strain image with 2D DP method. (C) Siemens EI B-mode and (D) strain image. (E) 9.4 Tesla *ex-vivo* MRI image. Benign solid (arrow) and soft nodules (dashed arrow), urethra, and peripheral tumor (circle).

Multiple lesions (six malignant and two benign) were identified by elastography and then validated by pathology report and MRI scans (Table 1). The appearance of the lesions on B-mode images did generally not allow for size measurements. Measured on the elastogram, the size of the lesions was generally bigger than was pointed by the MRI scans (Table 1). One reason is that the freehand palpation directions did not always identically match the MRI scan axes. On the other hand, elastography was closer in its estimates to the histological findings, which leads us to believe that certain parts of the lesions which looked benign on the MRI scans were actually correctly identified as hard tissue of cancer by the DP elastography method.

Specimen #1 presented multiple hard and soft lesions. Figure 3 (e) represents an *ex-vivo* T2-weighted coronal image from specimen MRI obtained at 9.4 Tesla. It shows detailed anatomy of the heterogeneous central gland with a solid nodule (arrow) representing benign prostatic hypertrophy (BPH), as confirmed by the pathology report. Elastography was able to detect this solid nodule despite the heterogeneity of the prostate, both with the Siemens method (Figure 3 (c), (d) - solid arrow), and with the 2D DP method (Figure 3 (a), (b) - solid arrow). *Ex-vivo* T2-weighted 9.4 Tesla coronal image from specimen MRI (Figure 3 (e)) also shows a soft nodule (dashed arrow) and a hypointense nodule in the left peripheral zone of the prostate (circle) documented to represent prostate cancer on pathology. Elastography in the corresponding areas showed hard tissue reflecting the high cellular density within the prostate cancer (Figure 3 (a) - circle).

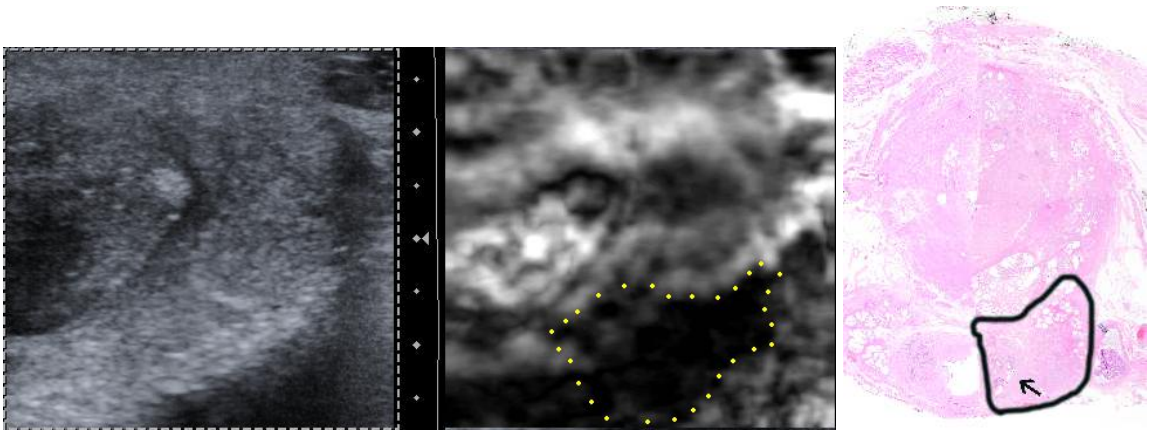

(a) (b)

Figure 4. Axial section of prostate specimen #1. (a) Left lateral section of the prostate's base; Siemens EI B-mode and strain image; hard lesion is outlined. (b) Hematoxylin & eosin stained histologic section of prostate base. The tumor (Gleason score 3+5 = 8, outlined in black) extended beyond the prostatic capsule in this section and invaded the left seminal vesicle (arrow).

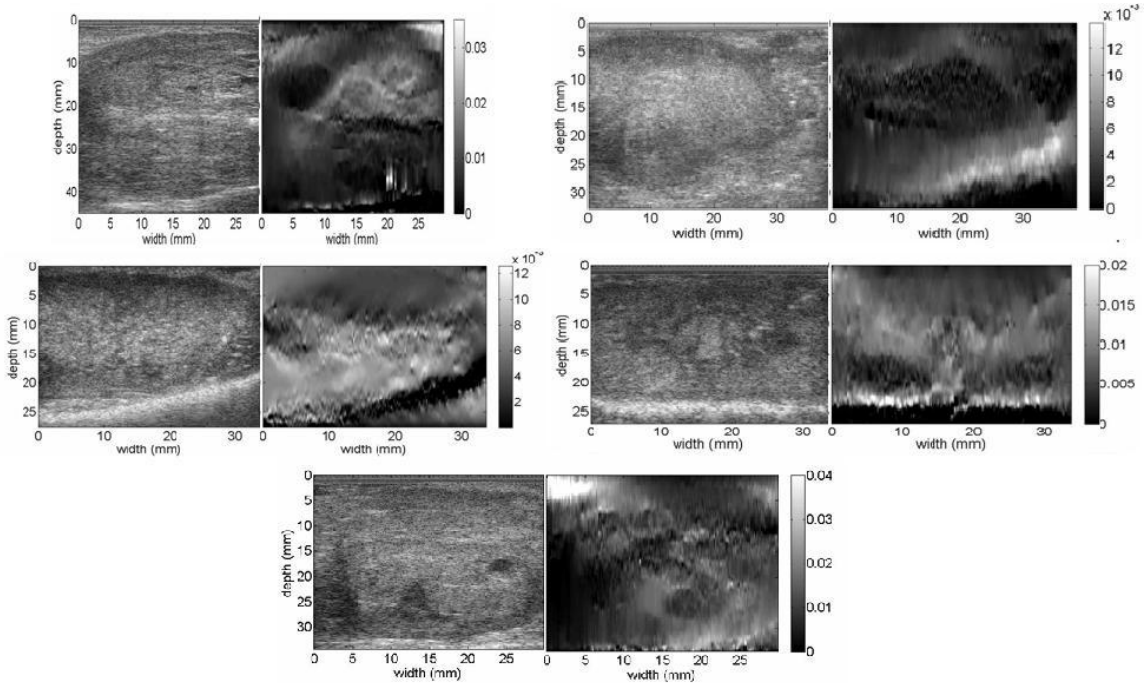

Figure 5. B-mode image (left) and freehand palpation strain image with 2D DP method (right) from specimens 1-5. Dark regions at the very bottom of elastograms represent structures outside the prostate tissue (e.g. operating table). The border of the prostatic tissue can be easily noticed as a highly reflective band at the bottom of B-mode images.

The axial sections acquired were also compared with histologic cross-sections, considered to be the gold standard. The prostate, submitted for histologic processing in four quadrant sections, has been digitally realigned to reconstruct a full histologic cross-section (Figure 4 (b)). For prostate specimen #1, a tumor with Gleason score of 8 was observed at the prostate base, left side. Ultrasound B-mode is not enough to identify the tumor, but elastography was able to detect it (Figure 4 (a)).

Specimen #2 presented a larger peripheral tumor which infiltrated the tissue outside the prostatic capsule . A similar infiltrated large mass was identified in specimen #3. Specimen #4 presented 2 (two) relatively small malignant masses localized in the peripheral zone towards the apex of the gland, while specimen #5 exhibited one large peripheral zone malignant tumor, which stretched on the entire right side of the gland, from the base, through the mid section and to the apex (Figure 5).

With respect with our DP elastography algorithm, we noticed that tumors (hard or soft) and the urethra are more clearly visible in the elastogram, compared to the B-mode image. We noticed that the 2D DP method is able to generate low-noise elastograms using two frames belonging to the same compression or relaxation part of the palpation excitation, even at compression rates up to 10%.

Figure 6. Laparoscopic ultrasound (LUS) probe.

Imaging human prostate specimens *ex-vivo* was the first step in evaluating ultrasound elastography for use in a laparoscopic procedure. Currently available LUS probes have either a straight or sometimes bent, flexible tip (Figure 6) housing the imaging hardware. A guidewire is sometimes used to deploy the probe in the desired area and position. The next step in the evaluation of ultrasound elastography technology will make use of a LUS probe. Using *ex-vivo* prostate specimens we will attempt to investigate palpation with a LUS probe, as well as optimal scan line locations in order to achieve lesion mapping with the least amount of added time to the surgical procedure.

4.2 Imaging cavernous nerves using an animal model

To our knowledge, the size of the human cavernous nerves has not been reported in the literature; anecdotal evidence estimates them to be 2-4 mm outer diameter. The sural nerve has been previously used as a graft for damaged cavernous nerves;[24,25] it is reportedly 2-3 mm in outer diameter.[26] The rat model has been reently used to study the cavernous nerves.[27,28] Fried et al found the rat cavernous nerve to be 500-1000 μ meters in width and 250-500 μ meters in depth.[27] Despite the smaller size, the rat model is well suited for ultrasound imaging because the rat cavernous nerve and ganglion are distinct structures, positioned superficially on the prostate gland, easy to visualize and scan (Figure 7 (a)). The cavernous nerve in rat however, has very little surrounding vessels or fat tissue. This is a disadvantage of the rat model; in human the cavernous nerves are part of the neurovascular bundle and the prostatic nervous endings are also covered by the fat and the prostatic capsule.

Anesthesiologists have long used ultrasound B-mode for nerve imaging to increase success in nerve blocking procedures. Literature reports about nerve appearance in B-mode ultrasound are often contradictory. Nerve roots like the cervical or brachial plexus, have a monofascicular, hypoechoic appearance.[29] Peripheral nerves

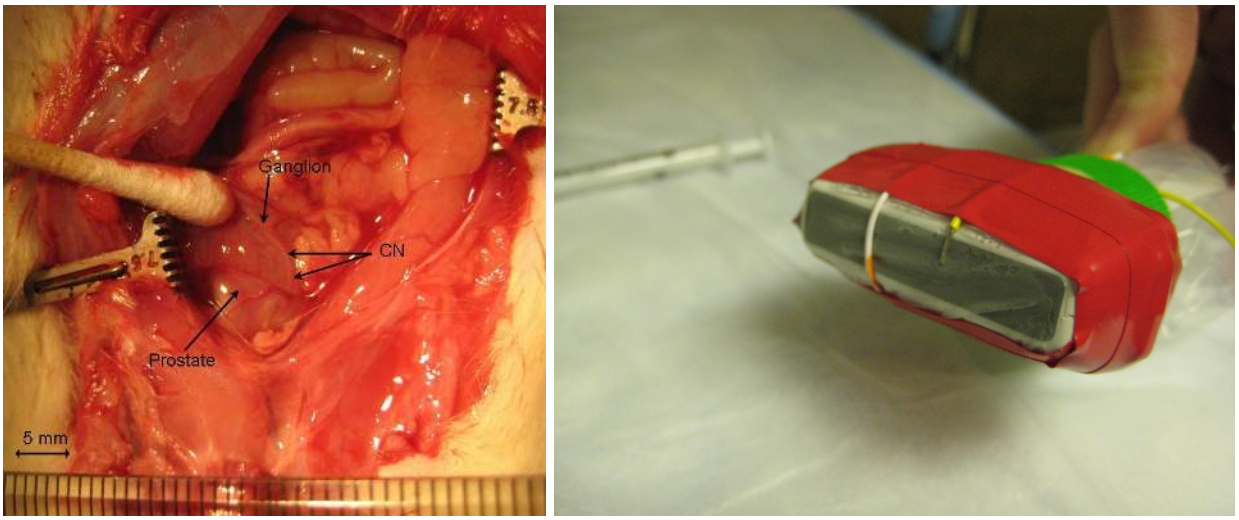

(a) (b)

Figure 7. Close-up view of prostate gland, cavernous nerve (CN) and ganglion in rat model (a). Ultrasound probe setup (b).

like the sciatic or the median nerve appear on a transverse scan as a collection of hypoechoic fascicles encased in a hyperechoic sheath, often referred to as the "'honeycomb"' mark.[30–33] No reports have been made so far as to the appearance of cavernous nerves on B-mode ultrasound, in either humans or other animal models. Our experience suggests that, given the small size of these structures, they usually appear hyperechoic, depending on size and orientation in the scanning plane (Figure 8).

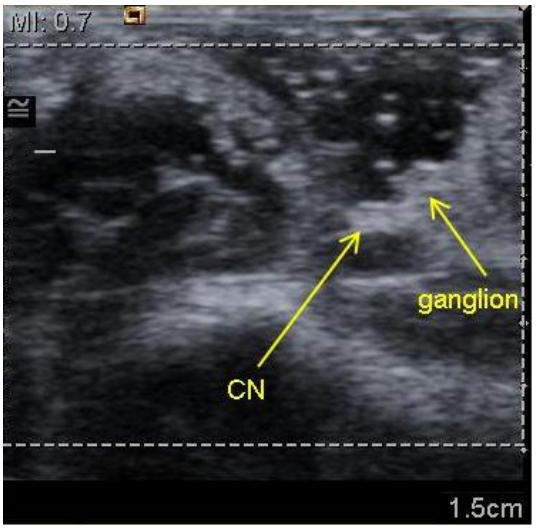

Figure 8. Cavernous nerve (CN) and ganglion in rat model. B-mode ultrasound: hyperechoic appearance (a) and hypoechoic appearance (b)

During our animal study, exposed cavernous nerves were initially identified visually. Validation was one of challenges we encountered, as it was very hard to confirm their identity by scanning along the course of the nerves. A pair of thin wires and a multimeter was used to create an electrical circuit on contact (Figure 7 (b)). Using this setup we were able to point out the nerve or ganglion while imaging. Ultrasound B-mode, RF,

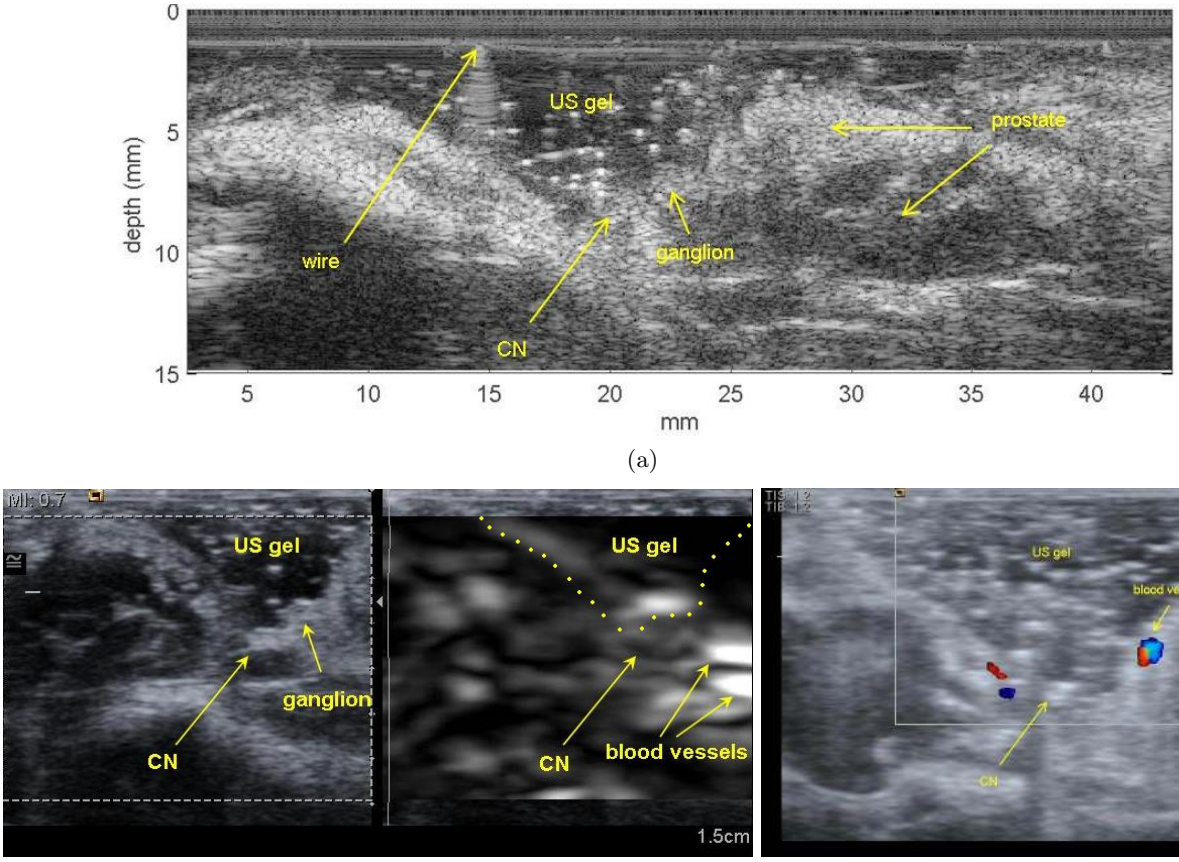

Figure 9. Cavernous nerve (CN), ganglion and vasculature in rat model. B-mode ultrasound (a), Siemens EI module with B-mode and strain image (b) and color Doppler ultrasonography (c).

elastography and color Doppler data were recorded from the animal subjects. RF acquisition was conducted using a Siemens Antares US scanner with an ultrasound research interface (URI) to access raw RF data. A Siemens VF 13-5 linear array (at 10MHz and a sampling rate of 40MHz) was used to acquire data using manual handling. Freehand palpation was performed on each exposed cavernous nerve. Our preliminary results show that elastography adds information about the nerve structure (Figure 9 (b)). As expected, nerves are harder, virtually non-compressible structures with respect to the surrounding structures. Elastography also improves differential diagnosis with the adjacent vessels (Figure 9 (c)). As compression is performed, nerves appear harder than the easily compresible neighboring vessels; color Doppler data validated the identification of neighboring vasculature (Figure 9 (c)).

Real-time imaging of cavernous nerves is an important part of achieving a successful nerve-sparing radical prostatectomy. Our preliminary results in an animal model are encouraging. We intend to continue our study as more controlled experiments are needed. A different animal model might be pursued in the future in an effort to better represent operating room conditions, where human cavernous nerves are surrounded by fat, vasculature and prostatic capsule. We also intend to evaluate the optimal ultrasound frequency needed to assure better confidence and resolution for nerve imaging. Evaluation of current LUS probes is a natural next step in this research area.

5. ACKNOWLEDGMENTS

The authors would like to acknowledge the support provided by Dr. Shelby Brunke from Siemens Medical Solutions USA, Inc. Ultrasound Division.

6. CONCLUSION AND FUTURE WORK

In the paper we took the first steps in evaluating ultrasound elastography as an enabling technology for image guided laparoscopic robotic prostatectomy. Elastography as a technology was chosen as it allows for real-time acquisition of images of the prostate gland, can be miniaturized and incorporated into robot-assisted prostatectomy and similar to human palpation, allows for contact based interrogation of the prostate gland surface. Our 2D DP technique proved consistent in the identification of lesions; hard and soft, malignant and benign, located in the prostate's central gland or in the prostate peripheral zone. The results were validated by the pathology of human prostatectomy specimens, as well as by *in vivo* and *ex vivo* MRI findings. We also evaluated for the first time the use of elastography in identifying small nervous structures. Preliminary results from a cavernous nerves rat model were encouraging as well. The experiments' success with elastography performed on *ex vivo* human prostate specimens and on cavernous nerves in animal model encourages us to pursue further the evaluation of this technique as an *in vivo* imaging technology guiding laparoscopic and robot-assisted prostatectomies.

REFERENCES

[1] Jemal, A. and et al, "Cancer statistics, 2007," *Cancer J. Clin.* **57**, 43–66 (2007).

[2] Bill-Axelson, A. and et al, "Radical prostatectomy versus watchful waiting in early prostate cancer," *New England Journal of Medicine* , 1977–1984 (2005).

[3] Box, G. and Ahlering, T., "Robotic radical prostatectomy: long-term outcomes," *Current Opinion Urology* **18**, 173–179 (March 2008).

[4] Ficcara, V. and et al, "Evidence from robot-assisted laparoscopic radical prostatectomy: A systematic review," *European Urol.* **51**, 45–56 (2007).

[5] Berrryhill, R. and et al, "Robotic prostatectomy: A review of outcomes compared with laparoscopic and open approaches," *J. Urol.* (in press 2008).

[6] Walsh, P., Lepor, H., and et al, "Radical prostatectomy with preservation of sexual function: anatomical and pathological considerations," *Prostate* **4**(5), 473–485 (1983).

[7] Ukimura, O. and et al, "Real-time transrectal ultrasonography during laparoscopic radical prostatectomy," *J Urol* **172**, 112–118 (2004).

[8] Ukimura, O. and et al, "Real-time transrectal ultrasound guidance during laparoscopic radical prostatectomy: Impact on surgical margins," *J. Urol.* **175**, 1304–1310 (2006).

[9] Coley, C. and et al, "Early detection of prostate cancer. part i. prior probability and effectiveness of tests. the american college of physicians," *Ann. Intern. Med* **126**(5), 394–406 (1997).

[10] Danhert, W. and et al, "Prostatic evaluation by transrectal sonography with histopathologic correlation: the echopenic appearance of early carcinoma," *Radiology* **158**, 97–102 (1986).

[11] Costello, A. J. and et al, "Anatomical studies of the neurovascular bundle and cavernosal nerves," *BJU Int.* **94**, 1071–1076 (2004).

[12] Su, L.-M. and et al, "Nerve-sparing laparoscopic radical prostatectomy: Replicating the open surgical technique.," *J. Urol.* **6**(1), 123–127 (2004).

[13] Lepor, H. and et al, "Precise localization of the anatomic nerves from the pelvic plexus to the corpora cavernosa: a detailed anatomical study of the adult male pelvis.," *J. Urol.* , 133–207 (1985).

[14] Pesavento, A. and Lorenz, A., "Real time strain imaging and in-vivo applications in prostate cancer.," *Ultrasonics Symp.* **2**, 1647–1652 (2001).

[15] Leven, J. e. a., "Davinci canvas: A telerobotic surgical system with integrated, robot-assisted, laparoscopic ultrasound capability.," *MICCAI* , 811–818 (2005).

[16] Garra, B., Céspedes, E., Ophir, J., Spratt, S., Zuurbier, R., Magnant, C., and Pennanen, M., "Elastography of breast lesions: initial clinical results," *Radiology* **202**, 79–86 (1997).

[17] Ophir, J. and et al, "Elastography: ultrasonic estimation and imaging of the elastic properties of tissues.," *Annu. Rev. Biomed. Eng.* **213**, 203–233 (1999).

[18] Pesavento, A., Perrey, C., Krueger, M., and Ermert, H., "A time-efficient and accurate strain estimation concept for ultrasonic elastography using iterative phase zero estimation," *IEEE Trans. Ultrason. Ferroelectr. Freq. Control* **46**, 1057 – 1067 (Sept. 1999).

[19] Lindop, J., Treece, G., Gee, A., and Prager, R., "Phase-based ultrasonic deformation estimation," *Ultrasonics, Ferroelectrics and Frequency Control, IEEE Transactions on* **55**, 94–111 (January 2008).

[20] Pellot-Barakat, C., Frouin, F., Insana, M., and Herment, A., "Ultrasound elastography based on multiscale estimations of regularized displacement fields," *IEEE T. Med. Imag.* **23**(2), 153–163 (2004).

[21] Rivaz, H., Boctor, E., and et al, "Ultrasound elastography: a dynamic programming approach," *IEEE Trans. Medical Imaging* **27**, 1373–1377 (October 2008).

[22] Jiang, J. and Hall, T., "A regularized real-time motion tracking algorithm using dynamic programming for ultrasonic strain imaging," in [*IEEE Ultrasonics Symp.*], 606–609 (October 2006).

[23] Bellman, R., [*Applied dynamic programming*], Princeton U. Press (1962).

[24] Kim, E. D. and et al, "Interposition of sural nerve restores function of cavernous nerves resected during radical prostatectomy..," *J. Urol.* **161**(1), 188–192 (1999).

[25] Kim, E. D. and et al, "Bilateral nerve grafting during radical retropubic prostatectomy: Extended follow-up.," *Urology* **58**, 983–987 (December 2001).

[26] Tesfaye, S. and et al, "Arterio-venous shunting and proliferating new vessels in acute painful neuropathy of rapid glycaemic control (insulin neuritis).," *diabetologia* **39**, 329–335 (1996).

[27] Fried, N. and et al, "Imaging the cavernous nerves in the rat prostate using optical coherence tomography.," *Lasers in Surgery and Medicine* **39**(1), 36–41 (2006).

[28] Fried, N. and et al, "Optical coherence tomography of cavernous nerves: A step toward real-time intraoperative imaging during nerve-sparing radical prostatectomy.," *J. Urol.* **72**(1), 198–203 (2008).

[29] Martinoli, C., Bianchi, S., Santacroce, E., Pugliese, F., M. Graif, M., and Derchi, L., "Brachial plexus sonography: A technique for assessing the root level.," *Am. J. Roentgenology* **179**, 699–702 (September 2002).

[30] Heinemeyer, O. and Reimers, C. D., "Ultrasound of radial, ulnar, median, and sciatic nerves in healthy subjects and patients with hereditary motor and sensory neuropathies," *Ultrasound in Medicine and Biology* **25**(3), 481 – 485 (1999).

[31] Schafhalter-Zoppoth, I. and Gray, A. T., "Ultrasound guidance for ulnar nerve block in the forearm," *Regional Anesthesia and Pain Medicine* **28**(4), 335 – 339 (2003).

[32] Gray, A., Collins, A., and Schafhalter-Zoppoth, I., "Sciatic nerve block in a child: a sonographic approach.," *Anesth. Analg.* **97**, 1300–1302 (2003).

[33] Gray, A. T., "Ultrasound-guided regional anesthesia; current state of the art," *Anesthesiology* **104**, 368–373 (2006).